

Chapter 8

Thermal and Mechanical Properties (II): Spark Plasma Sintered Ti–6Al–4V Alloy Reinforced with Mullite-Rich Tailings for Production of Energy Efficient Brake Rotor



Daniel Ogochukwu Okanigbe , Shade Rouxzeta Van Der Merwe,
Abimbola Patricia Popoola, Olawale Moshood Popoola,
and Pretty Lindiwe Linda

8.1 Introduction

The method to increase the energy efficiency of automobiles can be implemented in a variety of ways [1–9]. For instance, it can be accomplished by lowering parasitic frictional losses in the engine and drive-train, as well as by lowering rolling resistance of the tires, while designing the shape of the vehicle to enhance lower aerodynamic drag [10–18]. The disadvantage of these methods for reducing drag is that they make cars more difficult to stop [18, 20, 21].

Brakes are used to help stop vehicles. A brake, then, is a mechanical device that prevents motion by soaking up energy from a moving system. It is used to slow

D. O. Okanigbe (✉)

Department of Chemical, Metallurgical and Materials Engineering, Faculty of Engineering and the Built Environment, Tshwane University of Technology, Pretoria, South Africa

Pantheon Virtual Engineering Solutions, Nigel, South Africa

e-mail: okanigbedo@tut.ac.za; okanigbeogochukwu@gmail.com

S. R. Van Der Merwe (✉)

Department of Mechanical and Mechatronics Engineering, Faculty of Engineering and the Built environment, Tshwane University of Technology, Pretoria, South Africa

e-mail: vandermerweR1@tut.ac.za

A. P. Popoola · P. L. Linda

Department of Chemical, Metallurgical and Materials Engineering, Faculty of Engineering and the Built Environment, Tshwane University of Technology, Pretoria, South Africa

O. M. Popoola

Centre for Energy and Electric Power, Tshwane University of Technology,
Pretoria, South Africa

down, halt, or prevent motion in a moving vehicle, wheel, or axle, and is most frequently performed using friction [22]. The brakes are a crucial component of a car because they provide all necessary stopping purposes [23]. There are two main categories of brake configurations:

1. Drum brakes, in which flat pads are pressed against a circle rotor that is attached to the wheel hub, and
2. Disc brakes, in which curved contact surfaces (or “shoes”) are forced outward against a circular drum’s inner diameter.

Disc brakes are typically a standard part of cars, as well as some types of lorries and buses [24–27]. Compared to drum/shoe type brakes, the rotor/pad configuration of disc brakes often exhibits superior resistance to fade (i.e., reduction in friction as a function of rise in brake temperature) [28]. To prevent thermal cracking and rotor distortion, compositional changes and heat treatments are also adjusted [29, 30].

Most disc brake rotors are commonly constructed of gray cast iron (GCI), which is typically 3.5% carbon- and additive-free [31–33]. Because to its high-melting point, excellent heat storage, castability, and machinability, damping capacity, and cost-effectiveness [34]. Due to its durable performance, GCI is still the material of choice for braking discs and rotors [35]. With GCI, brake emissions in the form of dust (a non-exhaust emission) and particulate matter that are harmful to human health are produced [36–41], but poor corrosion resistance and excessive wear of the brake disc material during service remain issues of concern [34]. In an effort to reduce weight, a number of lightweight alloys have been investigated as replacements; nevertheless, due to their low-melting point and high-intrinsic costs, their widespread application has been constrained [34].

To evaluate lightweight materials for new energy-efficient brakes, however, there is a requirement to look into a number of research initiatives [42–44]. Ceramic composites [44], graphite materials [45], composites based on aluminum [46–48], and composites based on titanium [49, 50] are a few possible materials that could be used for this purpose.

Numerous titanium-based materials’ tribological properties have been studied and described in literature [50–53]. This interest was partly sparked by recent studies that promise to lower the price of titanium’s raw materials and so make more applications economically viable [54]. Furthermore, titanium alloys have not seen much commercial use in brake rotors outside of specialized racing applications [53, 55]. However, due to their low density (7.4 g/cm³), good stiffness, relatively high strength, and resistance to corrosive attack by ice-melting salts, they have been given some consideration for use in automotive braking systems [56].

The metallurgy and processing of titanium alloys are well understood as a result of previous and current research and development activities [57–60]. Their tribological properties, however, are less well recognized. While there has been a lot of research on the fretting properties of titanium alloys, there have been relatively few studies that discuss the thermal stress, sliding wear, and friction of titanium alloys [61, 62]. According to the reports based on published works, titanium alloys are unlikely to be suitable rotor materials in the absence of surface modification,

particle additions, or coating [20, 54]. While titanium-based alloys have many benefits for brakes, they also have three significant drawbacks.

1. Titanium has a low-thermal conductivity compared to cast iron,
2. The material is unfamiliar to the automotive sector, and
3. Titanium parts are expensive.

In terms of braking function, pad material selection, and rotor design, thermal behavior is especially important [63–65]. Raw materials, processing, fabrication, surface treatment (if any), and machining are some of the cost-related factors. By including reinforcements [20, 54] to create a composite [66], it is possible to address some of these flaws in Ti-6Al-4V alloy.

In order to retain the matrix-reinforcement system in the compact form and to guarantee the desired shape and dimensions of products made of such materials, a composite matrix material is composed of a material that is the continuous phase and fills the gap between the reinforcement. In addition to distributing loads to the reinforcement and shielding it from harm or adverse environmental effects, a matrix is frequently essential for the chemical and thermal properties of a composite material.

Any metal, including ferroalloys, magnesium alloys, aluminum alloys, zinc alloys, silver alloys, nickel alloys, copper alloys, and titanium alloys, can be used as a matrix material.

In addition, it can be made of non-metal, a ceramic matrix (such as aluminum oxide, silicon carbide, aluminum nitride, graphite, cement, and chamotte), and an organic matrix made of polymeric materials (such as polypropylene, polycarbonate, polyesters, epoxide, and polyamide), or carbon [67–71]. A component with superior attributes—usually strength properties—than the matrix properties is added to a matrix (that is a reinforcement).

The role of a reinforcement in a composite is typically to ensure, among other things, the required rigidity, increased yield strength and strength at room temperature, to prevent the propagation of cracks and to alter matrix susceptibility to plastic deformations [67–71]. A reinforcement can be either in the form of fibers, particles, or elements with complex geometric characteristics and even such ordered spatially.

However, because reinforcement is a generic phrase, its function for some composite materials may not only enhance mechanical or tribological capabilities but also enhance certain physiochemical properties, such as electric, thermal, or magnetic properties. As a result, the reinforcement of Ti-6Al-4V alloy with aluminosilicates like mullite, which has improved thermal shock and thermal stress resistance due to low-thermal expansion, good strength, and interlocking grain structure properties, can reduce the effects of poor thermal and wear resistance when used as brake rotors [72–74].

Mullite, a key ingredient in aluminosilicate ceramics, has been used in pottery and refractories for thousands of years [75]. Mullite is an old material that is finding new applications in electronics, optics, high-temperature structural products, and more as our understanding of it advances [76]. Compared to the majority of other metal oxide compounds, including alumina, several of its high-temperature properties are superior [75–78]. The use of Ti-6Al-4V + 3Al₂O₃SiO₂ composite in the

production of brake rotors will undoubtedly be prevented by the high cost of raw materials, including metal powders like mullite that can act as reinforcement for Ti-6Al-4V alloy [54]. This is because Ti-6Al-4V is significantly more expensive than alternatives like steel and aluminum (Table 8.1).

As a result, it becomes necessary to get mullite from secondary resources like slags, slimes, or mullite-rich tailings (MRT) from density separation of waste copper dust (WCD) [79], not only promotes environmental sustainability but also reduces environmental pollution caused by non-biodegradable solid wastes, such as metallic solid wastes, and powdery materials, among others [79]. Additionally, the high cost associated with using Ti-6Al-4V alloy will be significantly reduced by using tailings rich in mullite to create Ti-6Al-4V + 3Al₂O₃2SiO₂ composite [54].

The manufacturing of Ti-6Al-4V-based composites, such as Ti-6Al-4V + 3Al₂O₃2SiO₂, is not without its challenges. These issues stem from the processing of Ti-6Al-4V composites' high affinities for nitrogen and oxygen, which impairs the ductility of the resulting Ti-6Al-4V products [80]. The processing of Ti-6Al-4V products must therefore be done in regulated, high-temperature, and vacuum environments if the bulk material's characteristics are to be protected and unaffected by interstitial components [81]. Due to this method, Ti-6Al-4V products are exceedingly expensive and have a small range of applications. Researchers have typically found spark plasma sintering (SPS) to be affordable and cost-effective, giving great energy conservation and efficiency over the traditional sintering methods [82–84]. SPS is a new, emerging, and advanced powder consolidation technology.

The method has continued to draw a lot of interest from researchers since it offers the option of high heating vs. fast cooling rates while sintering powders to full densification in a little period of time, under a low-vacuum atmosphere, and at significantly lower temperatures [85, 86]. The most common ultra-rapid sintering method used to create nanostructured materials, carbon nanotube-based composites, intermetallic compounds, amorphous materials, metal/ceramic matrix composites, highly porous and refractory metals/ceramics, functionally graded materials, and other advanced materials is the SPS technique [87, 88].

The Ti-6Al-4V alloy can therefore clearly play a more substantial role in the design of brake rotors with superior heat conductivity and mechanical qualities in light of the aforementioned. To achieve this, the price must be brought down. Investigating the thermal conductivity and mechanical characteristics of SPS Ti-6Al-4V+ 3Al₂O₃2SiO₂ composite, for the manufacturing of brake rotors, is one suggested strategy for reaching this goal; nevertheless, this study.

Table 8.1 Cost of titanium compared to competing automobile materials [54]

Item	Material (\$ per pound contained)			
	Steel	Aluminum	Magnesium	Titanium
Ore	0.02	0.10	0.01	0.30
Metal	0.10	0.68	0.54	2.00
Ingot	0.15	0.70	0.60	4.50
Sheet	0.30–0.06	1.00–5.00	4.00–9.00	8.00-

Key: Magnesium sheet is not commonly used. Castings are \$2.50–\$10.00 per pound

8.2 Problem Statement

The following are general discussions of brakes rotors as it pertains to challenges faced with the integrity and durability of structural materials used in its design:

1. Developing the design of cars to improve reduce aerodynamic drag has the consequence of making the vehicles more difficult to stop [19–21].
2. Due to its durable performance, GC) is still the material of choice for braking discs/rotors [35]. Weight, low-corrosion resistance, and excessive brake disc material wear throughout service remain topics of concern, but [34].
3. Using GCI as a brake disc or rotor material causes brake emissions in the form of dust and particulate matter, which are harmful to human health [36–41].
4. Due to the limitations of GCI as a material for brake rotor/disc design, new, energy-efficient brakes must be made of lightweight materials [42–44].

Although titanium alloy (Ti–6Al–4V) is used to create brake rotors that are lightweight, it also offers potential benefits in terms of its high strength, low density, high-fracture toughness, and great corrosion resistance. For effective operation while in service, there are still several limits that must be addressed. These restrictions include the following:

5. The use of titanium alloy (Ti–6Al–4V) as a lightweight material to construct brake rotors is constrained by its high fabrication and processing costs, limited heat conductivity, and poor wear resistance [20].
6. Because of their strong affinities for nitrogen and oxygen during processing, Ti–6Al–4V composites exhibit reduced ductility [80].

8.3 Research Objectives

8.3.1 Main Objective

This project's primary goal is to analyze the thermal conductivity and mechanical property of a composite made from SPS Ti–6Al–4V and MRT that will be used to make brake rotors.

8.3.2 Sub-Objectives

1. The four sub-objectives of ore sampling, ore preparation, characterization of MRT and determination of the true density of MRT are to be completed in order to meet the aim.
2. Ti–6Al–4V+MRT composites SPS process optimization.

3. Determine how compositional variation in the SPS Ti–6Al–4V+MRT composites affects thermal conductivity.
4. Analyze the impact of compositional change on the wear resistance of composites made from SPS Ti–6Al–4V and MRT.
5. For the thermal conductivity and wear resistance of SPS Ti–6Al–4V+MRT tailings composites, create the best predictive model possible.
6. As a suitable structural material for production brake rotors, SPS Ti–6Al–4V+MRT composites will be validated experimentally and by simulation of its thermal conductivity and wear resistance.

8.4 Research Hypotheses

The following can be hypothesized based on the model suggested to address the difficulties identified:

1. Reduced aerodynamic drag.
2. Improved brake rotor material resistance to corrosion and wear in use.
3. Improved thermal conductivity of the material used to make brake rotors.
4. Removal of non-exhaust emissions.
5. Lowered cost of manufactured material for brake rotors.
6. Improved material ductility of brake rotors.

8.5 Significance of Study

These areas will benefit from this research's successful conclusion:

1. Production of a brake rotor that supports the low-cost development of an energy-efficient car.
2. The sustainability of the earth, in spite of other deteriorating environmental variables, while offering mullite as a substitute natural resource for MRT-based surface exploration.
3. The creation of material for brake rotor design using a method of fabrication and processing that is both affordable and efficient.

8.6 Literature Review

8.6.1 Introduction

With the help of a brake—a mechanical device that prevents motion by collecting energy from a moving system—rolling resistance of tires can be reduced. The brakes are a crucial component of a car because they provide all necessary stopping purposes [23]. According to Dizdar et al. [90], GCI has traditionally been used to

make brake rotors because it has strong wear resistance and good thermal conductivity properties. However, a GCI brake rotor is hefty since GCI is thick in comparison to other materials. At least three factors make a hefty brake rotor undesirable:

1. A vehicle's overall weight is increased by a hefty brake rotor, which decreases fuel efficiency and raises emissions.
2. The vehicle weight below the springs, or the unsprung vehicle weight, includes brake rotors. Unsprung weight increases the “NVH” (also referred to as “noise, vibration, and harshness”) associated with vehicle operation. NVH often gets better when unsprung weight is lowered.
3. A vehicle component that needs to be rotated while in use is a brake rotor. As a result, a heavier brake rotor needs more energy to change its rotational speed.

Hence, researching for an alternative lightweight material that can be used to design energy efficient brake rotors is very important.

8.6.2 Theoretical Background

8.6.2.1 Titanium and Ti–6Al–4V Alloy

Lightweight materials titanium (Ti) and its alloys (Ti–6Al–4V alloy) are known for their superior mechanical qualities. Their high price relative to other lightweight materials like aluminum (Al), however, restricts their use for a variety of engineering applications; a notable illustration of this limitation is their use as a structural material for the construction of automobile brake rotors.

8.6.2.2 Mullite

Due to its high-temperature stability [91] and suitable properties like high-melting point, thermal shock resistance, excellent dielectric strength, and good creep resistance, and corrosion stability, mullite is an important ceramic material for both conventional and advanced structural applications.

Neveling [92] provided a breakdown of WCD deposition rate during copper pyrometallurgy at South Africa's copper mine. The chemical composition of WCD is detailed in Table 8.2 [93, 94] (Fig. 8.1).

8.6.2.3 Design of Brake Rotors

The brake assembly should be built with high strength, good corrosion resistance, low noise, light weight, good thermal conductivity, long durability, strong wear resistance, consistent friction, and an acceptable cost-to-benefit ratio in mind. The numerous kinds of braking rotors are depicted in Fig. 8.2. Drum brakes have curved contact surfaces that are forced against the internal diameter of a drum, while uniform pads in disc brakes press against a circular disc that is mounted to the wheel [95].

Table 8.2 Mineralogical composition of PC's WCD [93, 94]

S/N	Minerals	Chemical formulae	Weight (%)
1	Cuprospinel	$Cu_{6.88}Fe_{17.12}O_{32.00}$	24.34
2	Chalcopyrite	$Cu_{6.88}Fe_{4.00}S_{8.00}$	7.95
3	Mullite	$Al(Al_{0.69}Si_{1.22}O_{4.85})$	42.97
4	Gypsum	$Ca(SO_{4.00})(H_{2.00}O)_{2.00}$	11.69
5	Quartz	$SiO_{2.00}$	11.45
6	Magnetite	$Mg_{0.04}Fe_{2.96}O_{4.00}$	1.60

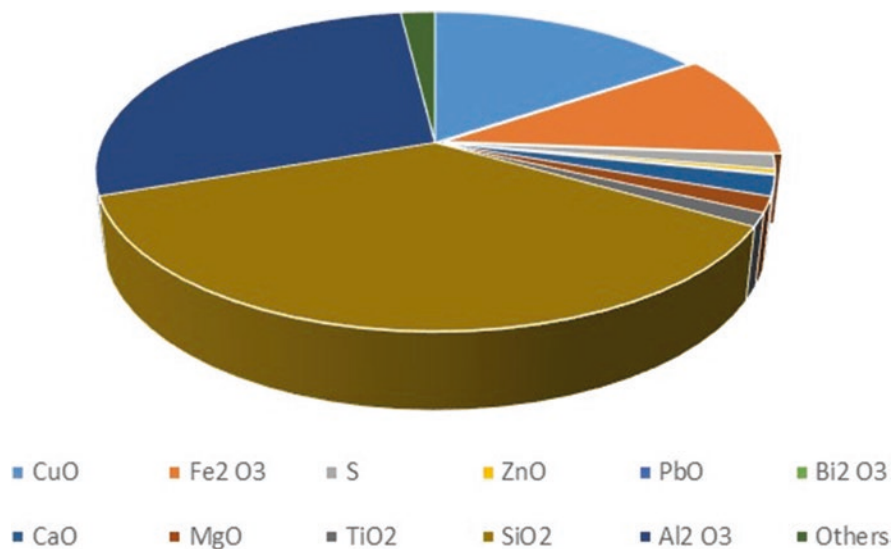


Fig. 8.1 Chemical composition of MRT as determined by X-ray fluorescence [123]

8.6.3 Review: Use of Ti–6Al–4V Alloy to Design Brake Rotors

Ti–6Al–4V alloy works, notably as a structural material for engineering applications in the automotive industry, as shown by the performance advantages that have been identified and extensively published in vehicle applications over many years [56]. The Ti–6Al–4V alloy has a high strength-to-density ratio and extraordinarily good corrosion resistance, according to the reports in the open literature [96–101].

Due to Ti and its alloys' remarkable corrosion resistance, they are used as brake pad guide pins and sealing rings in brake line connection flanges. As Ti has a limited thermal conductivity, the brake fluid is safeguarded [56].

In the conclusion section of their research, Froes et al. [56] stressed that Ti can unquestionably play a role in the development of fuel-efficient lightweight cars. The authors concede that there are methods that can be used to modify Ti–6Al–4V alloy in order to accomplish this goal (the creation of lightweight, fuel-efficient automobiles), but they caution that the method chosen must be economical.

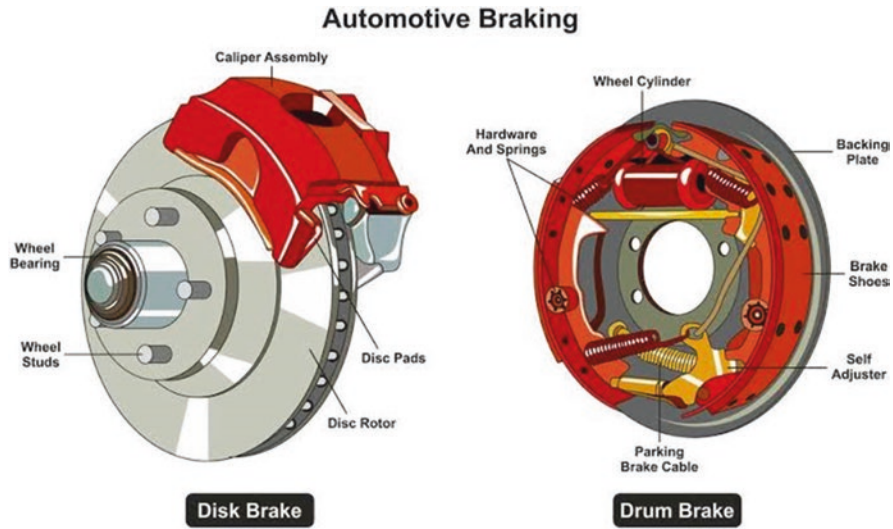


Fig. 8.2 Disk rake and drum brake (source: google image)

The authors concluded their report by stating that, given that 50 million cars and light trucks are produced around the world annually and that the current global titanium market is estimated to be worth 50,000 metric tons, even a small increase in titanium consumption per vehicle would have a significant impact.

However, it is vital to pinpoint the knowledge gap in order to develop a better Ti-6Al-4V matrix composite and construct resilient, energy-efficient automotive brake rotors. As a result, the parts that follow give a concentrated literature overview.

8.6.3.1 Problem Definition and Solution Formulation of Ti-6Al-4V Alloy for Design of Vehicle Brake Rotors

Problem Definition

The lifespan and performance of a vehicle's brake rotor are significantly influenced by the quality of the metal used in its construction. The brake rotor will function better on the car if a better material was chosen for its design. Ti-6Al-4V components that are lightweight can lighten the load on the vehicle, improving fuel efficiency [89]. However, Ti-6Al-4V alloy has a lower Young's modulus than steel and machining challenges in addition to other drawbacks like poor wear resistance and poor thermal conductivity [102, 103], an essential physical property that helps in the transfer of heat quickly and prevents thermo-mechanical fatigue, deformation, and hot cracking, thus prospering the applications of Ti-6Al-4V alloy in more complex or harsh conditions and improving the service life of engineering components desired.

Ti–6Al–4V alloy has only been used in a few high-end road vehicles and racing automobiles due to the high cost of metal alloy powders [56]. Ti–6Al–4V alloy is therefore unlikely to be a suitable structural material, especially in applications that emphasize weight-to-cost savings.

Solution Formulation

The automobile industry has previously set high financial and life cycle expectations, and the titanium sector has worked to accomplish these goals by concentrating on three key areas:

1. Enhanced wear resistance via Ti–6Al–4V alloy surface modification or coating.
2. Improved thermal conductivity achieved by using less expensive composite materials.
3. Investigating low-cost manufacturing techniques.

8.6.3.2 Additive Manufacturing of Ti–6Al–4V Alloy and Effect on Its Wear and Thermal Conductivity Properties as Material for Design of Brake Rotors

Because additive manufacturing is a low-cost production method, a recent trend in additive manufacturing of the Ti–6Al–4V alloy is to change the process parameters or add alloying elements to change the microstructure in order to get the desired performance.

Microstructural Modification of Ti–6Al–4V Alloy

Two-phase ($\alpha+\beta$) alloys with high strength are typically used in structural applications. These alloys' mechanical characteristics are highly dependent on their microstructure (geometrical arrangement of the two phases). Ti–6Al–4V is the most widely used of all $\alpha+\beta$ Ti alloys with Al as α phase (Fig. 8.3a) stabilizer and vanadium as a β phase (Fig. 8.3b) stabilizer [104].

As a result, the strong demand for new Ti–6Al–4V materials that perform well in severe settings has been sparked by developments in microstructural modification of Ti–6Al–4V alloy (such as the one brake rotors operate in). However, novel low-cost Ti–6Al–4V materials with improved wear resistance and thermal conductivity are in high demand, especially in the automotive sector, as a material to design brake rotors.

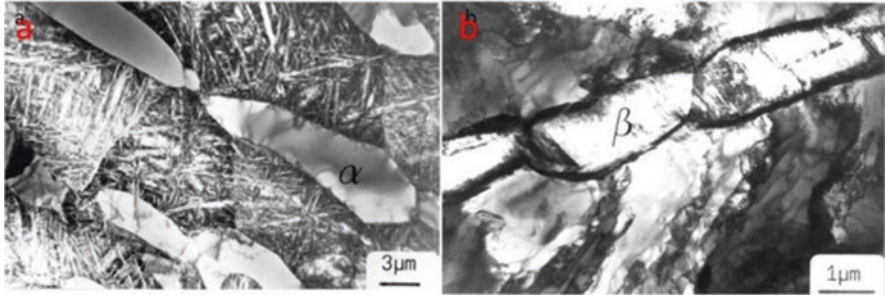


Fig. 8.3 TEM image of Ti-6Al-4V recrystallization to (a) bi-modal structure (950 °C) and (b) a globular structure [105]

Coating of Ti-6Al-4V Alloy

The low scratch and wear resistance of Ti-6Al-4V alloy, according to Yazdi et al. [106], can be improved by a diffusion treatment. Thermal oxidation at 850 °C for 3 and 6 h led to the formation of an oxygen diffusion layer (ODL) on Ti-6Al-4V. In comparison to Ti-6Al-4V alloy, the ODL Ti-6Al-4V samples shown greater hardness and less plastic deformation. When the ODL Ti-6Al-4V samples were subjected to normal loads of 40 N and 50 N, their brittle nature caused the development of cracks and substantial acoustic signals during scratching. The obtained results also indicated that ODL Ti-6Al-4V samples had stronger scratch and wear resistance than Ti-6Al-4V samples. However, oxygen enrichment would have a negative impact on the fatigue characteristics and consequently would not be appropriate for revolving brake rotors [107].

A vehicle brake rotor component was manufactured in the study by Martino [108] using a Ti base powder alloy that had been 3D printed to the correct shape before coating. On this 3D printed part, the wear surface coating was either plasma sprayed on or integrated into the body after the main component was created. Therefore, bond coat and topcoat are present on each braking surface. Typically, the topcoat is a ceramic layer made of zirconium oxide (65 to 75 parts by weight) and chromium carbide (25 to 35 parts by weight), with Al as an additional component in the bond coat. Less nickel and aluminum can be present in the topcoat and intermediate coat than in the bond coat.

After that, the combined product was subjected to sintering, machining, and double disc grinding. The enhanced rotor was made of two outer layers of Ti metal mixed with other metals, sandwiching a center layer made of Ti metal and metal alloy. This technology also offered a better way to create a vehicle brake rotor using 3D printing techniques.

Chromium and zirconium (\$10 per 100 g and \$15 per 100 g, respectively) are used in both case situations (i.e., [108, 109]), which defeats the purpose of a cost-effective strategy as suggested by Froes et al. [56]. As temperature decreases, the likelihood of the oxide layer detaching from the surface increases. This is due to the

significant mismatch between the lattices of titanium and metal oxide [110], the large ratio of the oxide to titanium specific volume [111], and the significant difference in the coefficients of thermal expansion between titanium and metal oxide [112].

In another study, Blau [20] tested a full-scale Ti rotor on a dynamometer to examine the potential of Ti-based materials as truck disc brake rotors. The designs for a commercial hydraulic truck rotor were used to create four full-sized, investment-cast Ti alloy rotors, which served the intended purpose. After that, a proprietary, ceramic-containing coating that was about 1–2 mm thick was thermally sprayed onto the rotors (Fig. 8.4a). They were put through standard industry tests to determine how well the Ti brake rotors performed.

According to the results, the Ti rotor ran hundreds of degrees Celsius hotter than the GCI under comparable circumstances. Figure 8.4b depicts the rotor's thermal picture. Due to previous laboratory testing and Ti's lower heat conductivity compared to Fe, maximum temperatures for thermally sprayed Ti rotor surfaces were higher than those for GCI. There was a time during the hot performance test portion when the pad ran the hottest and the rotor ran the coldest. The maximum lining temperature to maximum rotor temperature ratio for the series of sliding pairs reflects this. Then it was suggested that brake hardware made of Ti should not just be replaced with GCI using the same designs, but rather should be constructed to take these features into account. Better brake lining materials that are tailored for Ti-based rotors also need to be created and put to the test. In order to help transmit heat away, this will need to have a higher metallic content. It also needs to have acceptable wear lifetimes for both the pads and the rotors.

Reinforcement

According to Falodun et al. [104], the use of Ti–6Al–4V alloy is limited to temperatures about 400 °C because it loses effectiveness as wear resistance as temperature increases. The authors claim that the influence of reinforcing phases is responsible

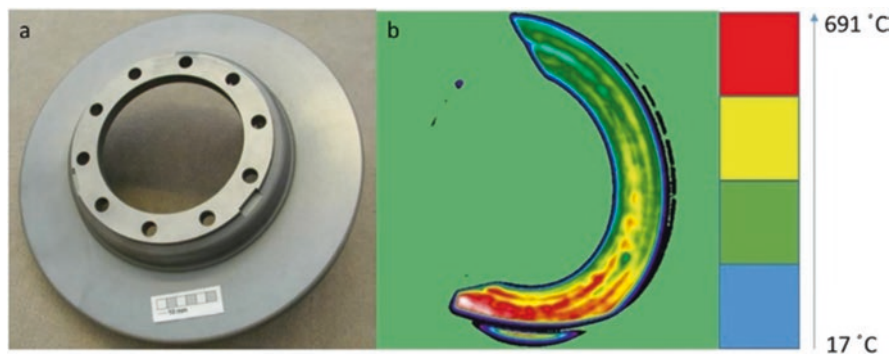


Fig. 8.4 (a) Ti alloy truck brake rotor with a protective thermally sprayed coating applied to the friction surfaces and (b) infrared image of a Ti-based brake rotor [20]

for the improved attributes of metal matrix composites (MMCs), including wear resistance and thermal conductivity, among others.

In the study by Patil et al. [113], optical microscopy, scanning electron microscopy (SEM), X-ray diffraction (XRD), electron back scattered diffraction, and pin-on-disk tribometry were used to examine the impact of adding TiB₂ to Ti-6Al-4V on the wear performance. The results demonstrated that the microstructure altered from martensite laths to a refined bi-modal structure with the addition of TiB₂. As a result, wear performance was improved. It is suggested that a slower cooling rate be used to create the bi-modal structure (Fig. 8.5) rather than the martensite structure that is typically seen in Ti-6Al-4V alloy treated with DMLS.

Thermal conductivity tests were made on unreinforced Ti and Ti-6Al-4V alloy, reinforced Ti with short fiber SiC, particulate SiC and particulate TiB₂, and reinforced Ti-6Al-4V alloy with long fiber SiC in the study done by Gordon et al. [115]. Instead of both forms of particle, the data obtained indicated an improvement in thermal conductivity with the TiB₂ reinforcement. The significant heat resistance of the SiC/Ti interface was cited as the cause of the anomaly and was linked to the type of reaction layer that was produced at the interface during processing. The high-thermal resistance of the interface also reduced the transverse conductivity of the Ti-6Al-4V reinforced with long SiC fibers, though in this instance the effect was less noticeable due to the reinforcement's larger diameter, which lowers the frequency at which heat must be transported across an interface. Finally, the short SiC fiber/Ti composite had comparable traits, with the exception that the axial

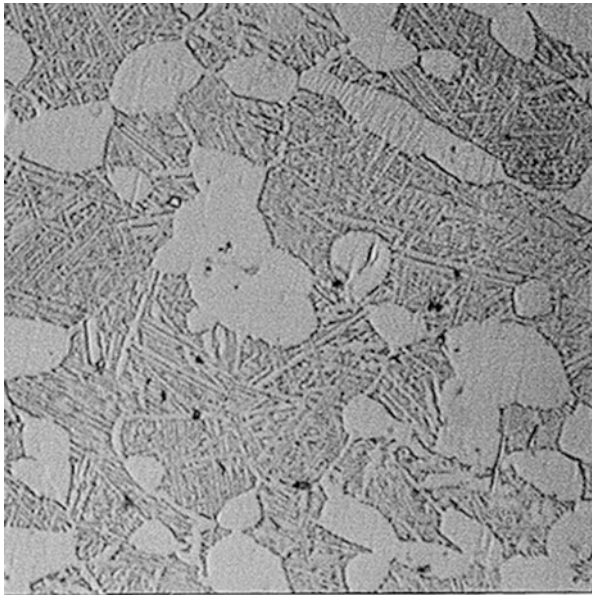


Fig. 8.5 The bi-modal microstructure when the globular α is surrounded by the Widmanstätten platelets [114]

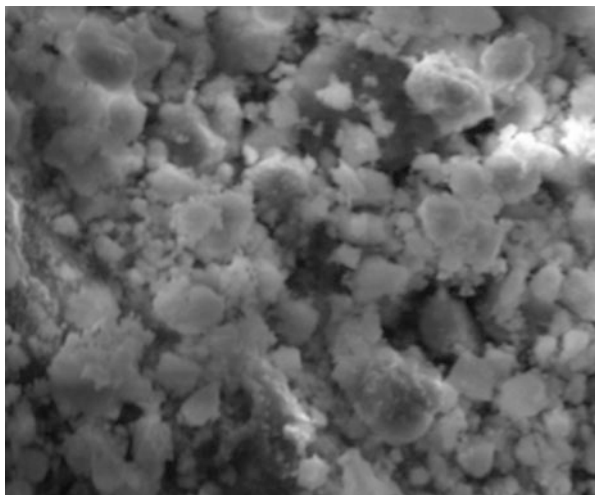


Fig. 8.6 Image of secondary resource of mullite from Palabora copper (PTY) company, Limpopo, South Africa. (Image taken by scanning electron microscopy)

conductivity was somewhat less than anticipated. This result was attributed to localized matrix porosity at the ends of the fibers.

The work of Kushch [116], which concentrated on the numerical algorithm of the multipole expansion approach for conductivity of ellipsoidal particle composite, is in accordance with Gordon et al. [115] and their study. The algorithm-based method, according to the authors, offers a quick and accurate analysis of the local potential fields and the effective conductivity of composites with a sufficient account for the arrangement and direction of inhomogeneities. According to the authors' findings, the volume content of inhomogeneities, their organization, size, and form (Fig. 8.6), inhomogeneity-matrix conductivity ratio, and normalized interface conductivity all affect an elliptic fiber composite's effective transverse conductivity [116]. The original cell shape was established as a perfect (square or hexagonal) fiber packing, imposing the porosity, or, alternatively, the number of fibers, mean fiber radius, and fiber volume fraction [117].

Secondary Resource of Mullite as Reinforcement to Ti-6Al-4V Alloy

Halloysite transforms to mullite (i.e., an aluminum silicate $3\text{Al}_2\text{O}_3 \cdot 2\text{SiO}_2$) during thermal processes, while in service as engine blocks, pistons, cylinders, and brake discs, according to Dobrzaski et al. [68]. This is why halloysite was chosen to develop aluminum porous skeletons (and, by extension, Ti porous skeletons), they reported. A sintered porous skeleton of Al or Ti alloy matrix composite materials created by gas-pressure infiltration processes will use the mullite as reinforcement.

However, it is anticipated that using inexpensive secondary resources, such as MRTs from density-separated copper smelter dust (Fig. 8.6), as reinforcement

material to either of these lightweight alloys will result in similar enhanced thermal conductivity properties without the need for phase transformation as in the case of the halloysite.

Ti and Ti–6Al–4V alloys have good physical and mechanical characteristics, with the exception of thermal conductivity and wear resistance, as was previously mentioned. Thus, low-cost processing equipment and raw materials such regular kaolinite or other clay minerals are required. The cost-effective method suggested by Froes et al. [56] can be achieved by using materials with high-thermal conductivity, such as mullite particles from secondary resources, such as MRT from density separated copper smelter dust, to manufacture Ti–6Al–4V-matrix composites.

Manufacturing Method

In the study by Tabrizi et al. [118], Ti alloy matrix composite reinforced by in-situ TiB whiskers (TiBw) and TiC particles were created by SPS fabrication of a powder combination consisting of Ti–6Al–4V and B4C at a temperature of 1100 °C (TiCp). For TiBw and TiCp, the reinforcement content in vol% ranged from 0.12 to 0.5 and from 0.5 to 2, respectively. The outcomes demonstrated the alignment of TiBw in the rolling direction of the rolled samples and the refining of alternative/lamellae. The Ti–6Al–4V–0.5 vol%, TiBw–0.12 vol% TiCp sample exhibited the maximum flexural yield strength, according to the findings of three-point bending tests (1850 MPa). It was discovered that the greatest flexural strength achieved by the Ti–6Al–4V–1 vol% TiBw–0.23 vol% TiCp composite was 2100 MPa after samples were subjected to a 66% reduction during hot rolling. Fractography analysis of the composite samples made using the SPS approach revealed that clustering of whiskers decreased flexural strength at greater reinforcing amounts.

Ti–6Al–4V foams were created by SPS employing a mixture of Ti–6Al–4V and NaCl powders in the works of Quan et al. [119]. The manufactured composite was unable to reach high-relative densities due to flaws (pores), which were present. The SPS was used to post-heat treat these sintered foams at 1100 °C for 5 min. While densifying the foam walls, these heat treatments were successful in reducing the micro porosity. The foams' Young's moduli ranged from 33.0 to 9.5 GPa, while their yield strengths ranged from 110.2 to 43.0 MPa and their porosity values ranged from 44.7 to 70.0%, all of which obeyed the Gibson–Ashby models. The post-heat treatment in a pressureless mode of the SPS at the stated 1100 °C for 5 min can be used to reduce the amount of porosity in pore-filled SPS-fabricated Ti–6Al–4V reinforced MRTs, even though these mechanical qualities appear unsatisfactory for brake rotor applications (TRMRT).

In the study by Adegebenjo et al. [120], which examined the densification, hardness, and tribological properties of Ti–6Al–4V reinforced by multi-walled carbon nanotubes (MWCNTs) compacts solidified by SPS. According to the authors, 1, 2, and 3 wt% MWCNTs were distributed in Ti–6Al–4V using high-intensity ball milling, and the powders from the milling process were then solidified using SPS at temperatures between 850 and 1000 °C. Ti–6Al–4V, MWCNTs, ground powders,

and the consolidated compacts were all characterized using SEM, transmission electron microscopy, and XRD as they were being received. On the Ti-6Al-4V and the Ti-6Al-4V/MWCNTs compacts sintered at 1000 °C, dry sliding wear tests were carried out at three load levels of 5, 15, and 25 N utilizing the ball-on-flat tribometer configuration with tungsten carbide (WC) as the counter face material. According to the findings, the relative density of compact Ti-6Al-4V/MWCNTs increased with higher sintering temperatures but decreased as more MWCNTs were added to the Ti-6Al-4V (Table 8.3). Vickers microhardness was improved by raising the sintering temperature and MWCNTs concentration. In comparison to unreinforced Ti-6Al-4V alloy, the wear volume loss and coefficient of friction for the compacts containing MWCNTs were improved [121].

Ti-6Al-4V alloy combines useful technical features, making it an intriguing material for the construction of vehicle brake rotors, according to Abe et al. [122]. The goal of the authors was to examine the effects of different refractory nitrides on the microstructure, mechanical, chemical, and high-temperature oxidation properties of Ti-6Al-4V. These nitrides included titanium nitride (TiN), hexagonal boron nitride (h-BN), and aluminum nitride (AlN). The three refractory nitrides as well as the Ti-6Al-4V powder were effectively combined using the SPS approach (AlN, TiN, and h-BN). SEM, optical microscopy, and XRD were used to analyze the SPS Ti-6Al-4V-based composites' microstructure and phase composition. According to the Archimedes principle and the Vickers microhardness tests, densification and microhardness of the test samples were measured.

The findings demonstrated that due to sufficient diffusional mass movement in strongly bonded particles at the matrix-reinforcement interfaces, the binary composites achieved close to full theoretical relative densification (i.e., 98.23%–99.54%). The relative densification (99.54%) and microhardness (7030 MPa) of the Ti-6Al-4V-3h-BN composite were ideal, exceeding those of the monolithic alloy by 200% and the Ti-6Al-4V alloy reinforced with AlN and TiN by roughly 48%, respectively. With AlN and TiN nanoparticle reinforcement, the matrix's yield and ultimate tensile strengths increased by about 47%, and with nano-h-BN reinforcement, they increased by 116%. In the high-temperature oxidizing environment, Ti-6Al-4V-3TiN demonstrated the highest resistance to oxidation with the least normalized weight gain of 0.85 mg/cm².

Table 8.3 Density and microhardness properties of Ti-6Al-4V and Ti-6Al-4V/MWCNTs compacts sintered at 1000 °C [120]

S/N	MWCNT content (wt%)	Theoretical density ^a (g/cm ³)	Measured density ^b (g/cm ³)	Relative density (%)	Microhardness (GPa)
1	0	4.43	4.41 ± 0.01	99.60 ± 0.03	3.55 ± 0.13
2	1	4.41	4.37 ± 0.01	99.10 ± 0.02	3.71 ± 0.09
3	2	4.38	4.31 ± 0.02	98.40 ± 0.04	3.88 ± 0.07
3	3	4.36	4.27 ± 0.01	97.90 ± 0.02	3.90 ± 0.05

Key: ^aRule of mixture (ρ Ti6Al4V $\frac{1}{4}$ 4.43 g/cm³ and r MWCNT $\frac{1}{4}$ 2.1 g/cm³)

^bArchimedes principle

Conclusion on Literature Review

The authors have determined from the studied literature that developing a vehicle's shape to reduce aerodynamic drag has the disadvantage of making the vehicle more difficult to stop. Additionally, authors concur that due to its durable performance, GCI is still the best material for brake rotors. However, the usage of GCI as a brake rotor material produces particulate matter that is harmful to human health and non-exhaust emissions. Due to the GCI's limitations as a material for brake rotor design, new, lightweight materials for energy-efficient brake rotors are required. The Ti–6Al–4V alloy is generally acknowledged by authors to be a deserving lightweight material for the design of energy-efficient brake rotors, despite its high cost, subpar thermal conductivity, and subpar wear resistance. However, in order to address the final two issues, numerous researchers have suggested that Ti–6Al–4V alloy be reinforced with ceramic elements like mullite (i.e., poor thermal conductivity and poor wear resistance). However, scholars concur that the price of metal powders, such as mullite and Ti–6Al–4V alloy, is too high to support the economics of the proposed composite (TRMRT). Although it has not been documented in the open literature, obtaining mullite from trash (i.e., a secondary supply of mullite) to accomplish this goal has the potential to be a cost-effective strategy. As a result, a knowledge gap has been found in the field of TRMRT for the manufacture of energy-efficient brake rotors. Therefore, it is suggested that future research efforts concentrate on examining the mechanical and thermal conductivity characteristics of SPS-TRMRT in order to produce brake rotors that are energy efficient.

8.7 Methodology

Due to its efficiency in terms of cost, it is possible to produce energy-efficient brake rotors by using secondary resources of mullite as reinforcement to Ti–6Al–4V. Therefore, the proposed methodology is described in this section.

8.7.1 Materials

8.7.1.1 Matrix Material

Titanium alloy will be the matrix material in this study (i.e., Ti–6Al–4V).

8.7.1.2 Reinforcement Materials

The MRT from the density separated WCD must be used as the reinforcing material. On Fig. 8.1, you can see the planned MRT's chemical compositions.

8.7.1.3 Equipment and Tools

The equipment/machine on Table 8.4 will be used for ample preparation or characterization during this proposed study.

8.7.1.4 Methods

Powder Weighing

The proposed Ti–6Al–4V + 3Al₂O₃2SiO₂ composite is made of the selected powders, which are 10, 20, and 30% by weight accordingly and are made of Ti–6Al–4V and tailings from the density separated copper smelting dust. Use an electronic scale to determine the weight of the amount.

Powder Mixing

A tube mixer will be used to properly combine the measured particles.

The mixed sample will be put into an SPS graphite die for a predetermined amount of time and at a predetermined temperature and pressure.

Density Measurement

Following sintering, the electronic densimeter will be used to measure density. We shall use Archimedes' principle to examine the effects of sintered composites.

Process Optimization

The percentage of Ti–6Al–4V alloy and MRT in the composite will be chosen as the two key parameters to be researched based on prior research and the literature. Three levels were selected for each parameter using the full factorial method (FFM),

Table 8.4 Equipment/machine for proposed study

S/N	Equipment/Machine	Purpose	Equipment/Machine	Purpose
1	Container mixer	SP	X-ray Diffractometer	CH
2	Rotating die splitter	SP	Scanning electron microscope	CH
3	SPS machine	SP	Energy dispersive spectroscope	CH
4	Grinding-polishing	SP	Electronic densimeter	CH
5	Stopwatch-tachometer	SP	Optical magnifying glass	CH
6	Electronic scale	SP	Hardness tester	CH

Key: *SP* Sample preparation, *CH* Characterization

Table 8.5 Experimental parameters and their relative levels

S/N	Parameters	Low (L)	Medium (M)	High (H)
1	Ti-6Al-4V	70	80	90
2	MRT	30	20	10

Table 8.6 Full factorial experimental design method for influencing factors and their levels coded with values in parenthesis

Tests	Percentage content of Ti-6Al-4V (%)	Percentage content of tailings (%)
1	L(70)	L(30)
2	L(70)	M(20)
3	L(70)	H(10)
4	M(80)	L(30)
5	M(80)	M(20)
6	M(80)	H(10)
7	H(90)	L(30)
8	H(90)	M(20)
9	H(90)	H(10)

as shown in Table 8.5. To carry out the experiment, an FFM was constructed taking into account the two factors (Table 8.5) and their pertinent three levels. Therefore, nine experiments will be carried out as given in Table 8.6. The relative levels of the parameters listed in Table 8.6 range from one (1) to three (3) levels. Interactions between parameters are not to be considered in this experiment.

Spark Plasma Sintering

The Ti–6Al–4V + 3Al₂O₃.2SiO₂ composite will be made using SPS technology.

For this, a predetermined volume of raw powder materials (Ti–6Al–4V, 3Al₂O₃2SiO₂) must be placed into a conductive graphite die. Then, under pulsed, low-voltage electric current flowing through the die assembly, mechanical pressure must be applied to the graphite die along the vertical axis. To track the sintering temperature while processing the powder, an optical pyrometer or thermocouple must be focused on the die outside wall.

Development of Predictive Models

Modeling Technique for Predictive Output

This sub-section presents the basic steps utilized in the modelling process as contained in this paper:

Step #1: Study trend of experimental samples.

Step #2: Set-up constraint models to categorize and group samples into sub-classes based on #1.

Step #3: Compute absolute difference between input and output samples in same class as grouped in #2.

Step #4: Identify different experimental levels for selected classes.

Step #5: Apply interpolant model to predict output.

Step #6: End.

Table 8.7 contains a generalized representation of the modelling variables. These variables were built into a model and used for the determination of the predictive outputs of the different mineral constituents as contained in the experimental concentrates. The modelling procedure herein is premised on constrained interpolation of outputs from any three sequenced experimental samples. Usually, two of these outputs are known via experimentation, while the third unknown output is obtained via predictive modelling. In Table 8.7, the first and second columns represent the sequenced experimental trials under consideration for interpolation. The third and fourth columns, respectively, represent the (%) proportions of the inputs (p_{i1} , p_{i2} , and p_{i3}) and outputs (p_{o1} , p_{o2} , and p_{o3}) for the mineral constituents under investigation. Furthermore, column five represents the experimental levels, while column six represents the absolute difference between the input and output values expressed in terms of Φ_1 , Φ_2 , and Φ_3 for each of the three experimental samples under consideration.

The following under listed are modelling notations as presented in this research:

$$\text{Output} = f(\text{speed, flow rate, input, feed rate, liquid solid ratio})$$

Let: serial number for inputs: $s_i = \{1, \dots, n - 1, n\}$ and serial number for outputs: $s_o = \{1, \dots, n - 1, n\}$ for $\forall n \in R$

where:

$$\text{exp}_{(i)i,j} = \text{Experimental inputs}$$

$$\text{exp}_{(o)i,j} = \text{Experimental outputs}$$

$$\text{Pre}_{(o)i,j} = \text{Predictive outputs}$$

$$p_{ij} = \% \text{input proportion of selected samples}$$

Table 8.7 Generalized representation of model variables

Level	Data acquisition procedure	Input value for variant factor p_{ij}	Output value for variant factor p_{oj}	Expt. levels	Absolute difference between p_{ij} and p_{oj}
1-First	Prediction	p_{i1}	p_{o1}	ξ	$ p_{i1} - p_{o1} = \Phi_1$
2-second	Experiment	p_{i2}	p_{o2}	μ	$ p_{i2} - p_{o2} = \Phi_2$
3-Third	Experiment	p_{i3}	p_{o3}	σ	$ p_{i3} - p_{o3} = \Phi_3$

p_{oj} = %output proportion of selected samples

$\Delta p_j = |p_{ij} - p_{oj}|$ absolute difference between p_{ij} and p_{oj}

where $j = \{1, \dots, k - 1, k\}$ represents the experimental levels.

The “absolute difference” models defined in terms of the experimental levels are shown in Eqs. (8.1), (8.2), and (8.3), and the final computational models for projecting the unknown outputs are shown in Eqs. (8.4), (8.5), and (8.6) with respect to Table 8.8.

$$\Phi_1 = \left[\frac{\Phi_3(\mu - \xi) - \Phi_2(\mu - \xi) - \Phi_2(\sigma - \mu)}{(\mu - \sigma)} \right] \tag{8.1}$$

$$\Phi_2 = \left[\frac{\Phi_3(\mu - \xi) + \Phi_1(\sigma - \mu)}{(\sigma - \mu) + (\mu - \xi)} \right] \tag{8.2}$$

$$\Phi_3 = \left[\frac{\Phi_1(\mu - \sigma) + \Phi_2(\sigma - \mu) + \Phi_2(\mu - \xi)}{(\mu - \xi)} \right] \tag{8.3}$$

$$|p_{i1} - p_{o1}| = \Phi_1 \tag{8.4}$$

$$|p_{i2} - p_{o2}| = \Phi_2 \tag{8.5}$$

$$|p_{i3} - p_{o3}| = \Phi_3 \tag{8.6}$$

Hence, $\Delta p_j = \Phi_j$.

Experimental Validation and Simulation

The metal matrix composite’s thermal conductivity and wear resistance will be experimentally determined in order to validate the expected ideal composition of Ti-6Al-4V + 3Al2O32SiO2.

Characterization and Tribological Measurement

Characterization

1. Scanning Electron Microscope (SEM) with Energy Dispersive Spectroscopy (EDS)

To ascertain the phase composition of the produced sample, the SEM/EDS shall be employed.

2. X-Ray Diffractogram (XRD)

To ascertain the phase composition of the produced sample, an X-ray diffractometer with monochromatic Cu K radiation must be used.

3. Microstructural Analysis

The microstructure of the produced composites will be assessed using an optical microscope and an electron microscope.

Tribological Measurement

The DUCOM TR 20-M-106 pin-on-disk sliding tribometer will be used to test the wear and frictional characteristics of the SPSed TARMRT in accordance with ASTM G99-05 standard (ASTM Standard, 2010). The disk samples will be loaded against the brake rotor material that has been cut into the shape of a square-headed pin while rotating at a predetermined revolution per minute (RPM). The tests will be run at various speeds of 2 and 3 m/s with a 65-N load over a 2000-m sliding distance. The pin will also be heated during the testing to a temperature of 2001 °C in order to mimic the effect of friction-induced heating during braking. The disk surface temperature will be gauged on-site using an infrared pyrometer (Omega OS550). The associated software will be used to continuously track changes in frictional force and depth of wear. Using an electronic balance with 0.1 mg precision, the weight loss of both the pin and the disk will be determined at the conclusion of each experiment. The coefficient of friction (Eq. 8.7), wear volume loss (Eq. 8.8), and wear rate (Eq. 8.9) will be calculated using the following equations based on the weight loss (Eq. 8.10) measurements and frictional force:

$$\text{Coefficient of friction } \text{CoF}(\mu) = \frac{F}{N} \quad (8.7)$$

$$\text{Wear volume loss } V_L (\text{mm}^3) = \frac{WL}{\rho} \quad (8.8)$$

$$\text{Wear rate } R (\text{mm}^3 / \text{Nm}) = \frac{VL}{N \times D} \quad (8.9)$$

$$\text{Wight loss } W_L (\text{g}) = W_I - W_F \quad (8.10)$$

where F is the frictional force (N), ρ the density of disk material (g/cm^3), N the normal load (N), D the sliding distance (m), W_I initial weight of the disk (g), and W_F = the final weight of the disk (g).

8.8 Contribution to Knowledge

The following information will be disclosed at the study's conclusion:

1. A new Ti-4Al-6V+ CSD tailings composite compositional blend is made available.

2. For improved heat conductivity and wear resistance of Ti–4Al–6V alloy, this compositional blend has not yet been used in the construction of braking rotors.
3. Consequently, the composition is brand-new.
4. The provision of mullite, a brand-new secondary resource.
5. Mullite is a secondary resource that has not been utilized as a ceramic material to improve the mechanical and thermal conductivity of Ti–4Al–6V alloy.
7. Consequently, the reinforcement material is fresh.

8.9 Ethical Considerations

This project has no unethical components.

8.10 Dissemination

The findings of this study will be published in publications recognized by the Department of Higher Education and Training (DHET), such as the ones listed below:

1. Reports in the Journal of Materials Science and Engineering, Publishers at Elsevier
2. Additive Manufacturing Journal, Publishers at Elsevier
3. Journal of Compounds and Alloy, Publishers at Elsevier, Materials Science Journal.
4. Publishers by Springer, Journal of OM, Publishers by Springer

The full article will be published in the conference proceedings, and the results will also be presented at regional and worldwide conferences.

8.11 Budget and Time Frame

8.11.1 Budget

Table 8.8 Estimated budget of the project

Items	Cost (R)	Source
Literature sourcing and stationaries	To be estimated	X
Materials and supplies	To be estimated	X
Analytical equipment	To be estimated	X
Travelling expenses	To be estimated	X
Miscellaneous expenses	To be estimated	X
Total		X

Key: *TUT* Tshwane University of Technology; *R* Rand

8.11.2 Time Frame (Table 8.9)

Table 8.9 Estimated time frame of the project

S/N	Task name	Year	
1	Proposal (compilation and presentation)	WIP	WIP
2	Literature review	WIP	WIP
3	Material sourcing	WIP	WIP
4	Sample preparation (sampling)	WIP	WIP
5	Fabrication of test samples optimization process	WIP	WIP
6	Fabrication of test samples	WIP	WIP
7	Thermal conductivity and wear resistance tests	WIP	WIP
8	Results, data, and analysis	WIP	WIP
9	Optimum predictive model development	WIP	WIP
10	3D print of brake rotor and validation of optimum prediction	WIP	WIP
11	Compilation and presentation of final report	WIP	WIP

Key: *WIP* work in progress

References

1. Y. Miao, P. Hynan, A. Von Jouanne, A. Yokochi, Current Li-ion battery technologies in electric vehicles and opportunities for advancements. *Energies* **12**(6), 1074 (2019)
2. D.X. Yang, L.S. Qiu, J.J. Yan, Z.Y. Chen, M. Jiang, The government regulation and market behavior of the new energy automotive industry. *J. Clean. Prod.* **210**, 1281–1288 (2019)
3. B. Tanç, H.T. Arat, E. Baltacıoğlu, K. Aydın, Overview of the next quarter century vision of hydrogen fuel cell electric vehicles. *Int. J. Hydrog. Energy* **44**(20), 10120–10128 (2019)
4. Y. Chen, J. Gonder, S. Young, E. Wood, Quantifying autonomous vehicles national fuel consumption impacts: A data-rich approach. *Transp. Res. A Policy Pract.* **122**, 134–145 (2019)
5. L.X. Hesselink, E.J. Chappin, Adoption of energy efficient technologies by households—barriers, policies and agent-based modelling studies. *Renew. Sust. Energ. Rev.* **99**, 29–41 (2019)
6. L. Zhou, Q. Fu, C. Huo, M. Tong, X. Liu, D. Hu, Mullite whisker-mullite/yttrium aluminosilicate oxidation protective coatings for SiC coated C/C composites. *Ceram. Int.* **45**(18), 24022–24030 (2019)
7. X. Qu, Y. Yu, M. Zhou, C.T. Lin, X. Wang, Jointly dampening traffic oscillations and improving energy consumption with electric, connected and automated vehicles: A reinforcement learning based approach. *Appl. Energy* **257**, 114030 (2020)
8. D. Phan, A. Bab-Hadiashar, C.Y. Lai, B. Crawford, R. Hoseinnezhad, R.N. Jazar, H. Khayyam, Intelligent energy management system for conventional autonomous vehicles. *Energy* **191**, 116476 (2020)
9. S. Thomas, J. Rosenow, Drivers of increasing energy consumption in Europe and policy implications. *Energy Policy* **137**, 111108 (2020)
10. D. Colavincenzo, F.V. Diaz, J. Geither, Bendix commercial vehicle systems LLC, 2020. Front end motor-generator system and hybrid electric vehicle operating method. U.S. Patent Application 16/689,343, 2020
11. D. Smith, B. Ozpineci, R.L. Graves, P.T. Jones, J. Lustbader, K. Kelly, K. Walkowicz, A. Birky, G. Payne, C. Sigler, J. Mosbacher, Medium-and heavy-duty vehicle electrification: An assessment of technology and knowledge gaps (No. ORNL/SPR-2020/7). Oak Ridge National Lab.(ORNL), Oak Ridge, TN (United States), 2020

12. Y.T. Shah, *Modular Systems for Energy Usage Management*. Boca Raton, Florida: CRC Press Taylor & Francis Ltd, 2020.
13. Y.Y. Wang, V.P. Atluri, D. Li, C.J. Lee, GM Global Technology Operations LLC, Coordinated torque and speed control systems and logic for hybrid electric vehicles. U.S. Patent 10,597,022, 2020
14. N. Bizon, *Optimization of the Fuel Cell Renewable Hybrid Power Systems* (Springer, Cham, 2020)
15. A. Mohanadass, Making the Most of the Energy We Have: Vehicle Efficiency. In: Quang Dinh T, ed. *Intelligent and Efficient Transport Systems - Design, Modelling, Control and Simulation* [Internet]. IntechOpen, 2020
16. J. Lee, K.P. Ha, J. Lee, K. Nam, A study on the design and development of an integrated 48V motor with motorized internal combustion engine (No. 2020-01-0446). SAE Technical Paper, 2020
17. A.M. Dudar, K. Miller, T.G. Leone, Ford Global Technologies LLC. Engine oil warm up using inductive heating. U.S. Patent 10,704,433, 2020
18. J.T. Dalum, Power technology holdings LLC. Hybrd vehicle drive system and method and idle reduction system and method. U.S. Patent Application 16/808,067, 2020
19. S.W. Baek, S.W. Lee, Aerodynamic drag reduction on a realistic vehicle using continuous blowing. *Microsyst. Technol.* **26**(1), 11–23 (2020)
20. P.J. Blau, Prospects for titanium-based materials as truck disc brake rotors. ORNL Tech Report, ORNL TM-2007-111, 2007
21. J.M.L. Jeyan, K.S. Nair, G. Vincent, CFD analysis on various commercial vehicles to evaluate the aerodynamic characteristics-a comparative study. *J. Adv. Res* **6**, 59 (2020)
22. A.P. Borse, Design and analysis of brake rotor (DISC), 2019
23. A. Kruczek, A. Stribrsky, A full-car model for active suspension-some practical aspects, in *Proceedings of the IEEE International Conference on Mechatronics, 2004. ICM'04*, (IEEE, 2004), pp. 41–45
24. L.F. da Cruz, C. Rudek, R.Z. Freire, Different approaches on how to improve braking performance in M3 vehicles to meet secondary brake requirements from ECE R13 regulation through low cost solutions (No. 2019-36-0011). SAE Technical Paper, 2020
25. N.V. Vetter, A.C. De Oliveira, E.H.S. Fontes, F. Nogueira, G.H. Fonseca, L.F.N. De Souza, R.D.O. Dos Reis, V.C. Manenti, Development challenges of hydraulic brakes for commercial vehicles (No. 2019-36-0013). SAE Technical Paper, 2020
26. G. Gopinath, P. Murali, Analysis of redesigned brake shoe. *Mater. Today Proc* **22**, 507–513 (2020)
27. A.Y. Tripariyanto, L.D. Indrasari, S.V. Widodo, A. Komari, Disc brake type of braking system on rear shaft of Go-kart Daiho 7.5 HP. *J. Phys. Conf. Ser.* **1569**(3), 032049 IOP Publishing (2020)
28. P.J. Blau, J.C. McLaughlin, Effects of water films and sliding speed on the frictional behavior of truck disc brake materials. *Tribol. Int.* **36**(10), 709–715 (2003)
29. P.J. Blau, B.C. Jolly, J. Qu, W.H. Peter, C.A. Blue, Tribological investigation of titanium-based materials for brakes. *Wear* **263**(7–12), 1202–1211 (2007)
30. W. Li, X. Yang, S. Wang, J. Xiao, Q. Hou, Comprehensive analysis on the performance and material of automobile brake discs. *Metals* **10**(3), 377 (2020)
31. A. Polak, J. Grzybek, The mechanism of changes in the surface layer of grey cast iron automotive brake disc. *Mater. Res.* **8**(4), 475–479 (2005)
32. R. Srivastava, B. Singh, K.K. Saxena, Influence of S and Mn on mechanical properties and microstructure of grey cast iron: An overview. *Mater. Today Proc* **26**, 2770 (2020)
33. I. Mutlu, O. Eldogan, F. Findik, Tribological properties of some phenolic composites suggested for automotive brakes. *Tribol. Int.* **39**(4), 317–325 (2006)
34. O. Aranke, W. Algenaid, S. Awe, S. Joshi, Coatings for automotive gray cast iron brake discs: A review. *Coatings* **9**(9), 552 (2019)
35. D.B. Miracle, Metal matrix composites—from science to technological significance. *Compos. Sci. Technol.* **65**(15–16), 2526–2540 (2005)

36. A. Thorpe, R.M. Harrison, Sources and properties of non-exhaust particulate matter from road traffic: A review. *Sci. Total Environ.* **400**(1–3), 270–282 (2008)
37. T. Grigoratos, G. Martini, Brake wear particle emissions: A review. *Environ. Sci. Pollut. Res.* **22**(4), 2491–2504 (2015)
38. J. Kukutschová, V. Roubíček, M. Mašláň, D. Jančík, V. Slovák, K. Malachová, Z. Pavlíčková, P. Filip, Wear performance and wear debris of semi metallic automotive brake materials. *Wear* **268**(1–2), 86–93 (2010)
39. T.A. Cahill, D.E. Barnes, N.J. Spada, J.A. Lawton, T.M. Cahill, Very fine and ultrafine metals and ischemic heart disease in the California Central Valley 1: 2003–2007. *Aerosol Sci. Technol.* **45**(9), 1123–1134 (2011)
40. L. Ntziachristos, P. Boulter, Road vehicle tyre and brake wear road surface wear. In: Joint EMEP/CORINAIR emission inventory guidebook, 3rd ed., european environment, agency, copenhagen, pp. B770-1–B770-25 (2003)
41. M. Penkała, P. Ogrodnik, W. Rogula-Kozłowska, Particulate matter from the road surface abrasion as a problem of non-exhaust emission control. *Environments* **5**(1), 9 (2018)
42. A. Mohan, S. Sripad, P. Vaishnav, V. Viswanathan, Trade-offs between automation and light vehicle electrification. *Nat. Energy* **5**, 1–7 (2020)
43. D.O. Ayogwu, I.S. Sintali, M.A. Bawa, A review on brake pad materials and methods of production. *Compos. Mater* **4**(1), 8 (2020)
44. M.A. Ts, M. Kt, Study and comparison of mechanical properties of brake rotors made of steel based hybrid metal matrix composite and grey cast iron, 2020
45. Y. Lyu, U. Olofsson, On black carbon emission from automotive disc brakes. *J. Aerosol Sci.* **148**, 105610 (2020)
46. A.A. Agbeleye, D.E. Esezobor, S.A. Balogun, J.O. Agunsoye, J. Solis, A. Neville, Tribological properties of aluminium- clay composites for brake disc rotor applications. *J. King Saud Univ. Sci* **32**(1), 21–28 (2020)
47. S.A. Paul, Honda Motor Co Ltd. Aluminum Ceramic Composite Brake Assembly. U.S. Patent Application 16/264,352, 2020
48. F.M. Firouz, E. Mohamed, A. Lotfy, A. Daoud, M.T. Abou El-Khair, Thermal expansion and fatigue properties of automotive brake rotor made of AlSi–SiC composites. *Mater. Res. Exp.* **6**(12), 1265d2 (2020)
49. N.K. Konada, K.N.S. Suman, Brake friction materials-a review. *I-Manager's J. Mater. Sci* **7**(4), 51 (2020)
50. B. Zheng, F. Dong, X. Yuan, Y. Zhang, H. Huang, X. Zuo, L. Luo, L. Wang, Y. Su, X. Wang, K. Shi, Evaluation on Tribological characteristics of (TiC+ TiB)/Ti–6Al–4V composite in the range from 25°C to 600°C. *Wear* **450–451**, 203256 (2020)
51. S. Gheorghe, C.I. Pascu, C. Nicolicescu, Titanium-based sintered alloy with improved wear resistance, in *Applied Mechanics and Materials*, vol. 896, (Trans Tech Publications Ltd., 2020), pp. 270–275
52. R. Yamanoglu, Network distribution of molybdenum among pure titanium powders for enhanced wear properties. *Metal Powder Report*, 2020
53. M.J. Donachie, *Titanium: a Technical Guide* 2nd ed. (ASM International: Materials Park, OH, 2000).
54. H. Friedrich, J. Kiese, H.G. Haldenwanger, A. Stich, Titanium in automotive applications–nightmare, vision or reality, in *Proceedings 10th World Conference on Titanium*, ed. by G. Lutjering, (Wiley–VCH, Weinheim, 2003)
55. V.A. Joshi, *Titanium Alloys: An Atlas of Structures and Fracture Features* CRC Taylor & Francis Group, Boca Raton, p 1–2, 2006.
56. F.H. Froes, H. Friedrich, J. Kiese, D. Bergoint, Titanium in the family automobile: The cost challenge. *JOM* **56**(2), 40–44 (2004)
57. M. Jackson, K. Dring, A review of advances. In processing and metallurgy of titanium alloys. *Mater. Sci. Technol.* **22**(8), 881–887 (2006)
58. L. Bolzoni, E.M. Ruiz-Navas, E. Gordo, Quantifying the properties of low-cost powder metallurgy titanium alloys. *Mater. Sci. Eng. A* **687**, 47–53 (2017)

59. I. Chang, Y.E.D.S. Zhao, *Advances in Powder Metallurgy: Properties, Processing and Applications* Vol 60 Woodhead Publishing, Oxford, 2013.
60. S. Bahl, S. Suwas, K. Chatterjee, Comprehensive review on alloy design, processing, and performance of β titanium alloys as biomedical materials. *Int. Mater. Rev.*, **66**, 114–139 (2020)
61. J.E. Allison, G.S. Cole, Metal-matrix composites in the automotive industry: Opportunities and challenges. *JOM* **45**(1), 19–24 (1993)
62. A.M. Sherman, C.J. Sommer, F.H. Froes, The use of titanium in production automobiles: Potential and challenges. *JOM* **49**(5), 38–41 (1997)
63. H.J. Cho, C.D. Cho, A study of thermal and mechanical behavior for the optimal design of automotive disc brakes. *Proc. Instit. Mech. Eng. Part D J. Automob. Eng.* **222**(6), 895–915 (2008)
64. A. Belhocine, O.I. Abdullah, Thermomechanical model for the analysis of disc brake using the finite element method in frictional contact. *Multiscale Sci. Eng.* **2**, 1–15 (2020)
65. A. Belhocine, A. Afzal, Computational finite element analysis of brake disc rotors employing different materials. *Aust. J. Mech. Eng.* **20**, 1–14 (2020)
66. A. Celotto, In situ tensile tests of additively manufactured and wrought Ti-6Al-4V alloys, 2020
67. A.K. Kaw, *Mechanics of Composite Materials* 2nd edition, CRC Press, Boca Raton, FL, USA, 2005.
68. L.A. Dobrzański, G. Matula, A.D. Dobrzańska-Danikiewicz, P. Malara, M. Kremzer, B. Tomiczek, M. Kujawa, E. Hajduczek, A. Achtelik-Franczak, L.B. Dobrzański, J. Krzyszczyk, Composite materials infiltrated by aluminium alloys based on porous skeletons from alumina, mullite and titanium produced by powder metallurgy techniques, in *Powder Metallurgy-Fundamentals and Case Studies*, (2017)
69. K.K. Chawla, Carbon fiber/carbon matrix composites, in *Composite Materials*, (Springer, Cham, 2019), pp. 297–311
70. B.O. Baba, S. Thoppul, R.F. Gibson, Experimental and numerical investigation of free vibrations of composite Sandwich beams with curvature and debonds. *Exp. Mech.* **51**(6), 857–868 (2011)
71. P.K. Hg, A. Xavier, Processing of graphene/CNT-metal powder, in *Powder Technology*, Intechopen, (2018), p. 45
72. L. Zhuang, Q.G. Fu, X. Yu, Improved thermal shock resistance of SiCnw/PyC Core-Shell structure-toughened CVD-SiC coating. *J. Eur. Ceram. Soc.* **38**(7), 2808–2814 (2018)
73. J.P. Zhang, Q.G. Fu, J.L. Qu, L. Zhuang, P.P. Wang, H.J. Li, An inlaid interface of carbon/carbon composites to enhance the thermal shock resistance of SiC coating in combustion environment. *Surf. Coat. Technol.* **294**, 95–101 (2016)
74. Y. Zhou, A. Ravey, M.C. Péra, A survey on driving prediction techniques for predictive energy management of plug-in hybrid electric vehicles. *J. Power Sources* **412**, 480–495 (2019)
75. D.J. Duval, S.H. Risbud, J.F. Shackelford, Mullite, in *Ceramic and Glass Materials*, (Springer, Boston, MA, 2008), pp. 27–39
76. J.F. Shackelford, R.H. Doremus, in *Ceramic and Glass Materials: Structure, Properties and Processing*. New York: Springer, (2008)
77. H. Schneider, J. Schreuer, B. Hildmann, Structure and properties of Mullite—A review. *J. Eur. Ceram. Soc.* **28**(2), 329–344 (2008)
78. C. Sadik, I.E. El Amrani, A. Albizane, Recent advances in silica-alumina refractory: A review. *J. Asian Ceramic Soc.* **2**(2), 83–96 (2014)
79. D. Okanigbe, P. Olawale, A. Popoola, A. Abraham, A. Michael, K. Andrei, Centrifugal separation experimentation and optimum predictive model development for copper recovery from waste copper smelter dust. *Cogent Eng.* **5**(1), 1551175 (2018)
80. A.O. Adegbenjo, P.A. Olubambi, J.H. Potgieter, E. Nsiah-Baafi, M.B. Shongwe, Interfacial reaction during high energy ball milling dispersion of carbon nanotubes into Ti6Al4V. *J. Mater. Eng. Perform.* **26**(12), 6047–6056 (2017)
81. M. Yan, W. Xu, M.S. Dargusch, H.P. Tang, M. Brandt, M. Qian, Review of effect of oxygen on room temperature ductility of titanium and titanium alloys. *Powder Metall.* **57**(4), 251–257 (2014)

82. N.S. Weston, F. Derguti, A. Tudball, M. Jackson, Spark plasma sintering of commercial and development titanium alloy powders. *J. Mater. Sci.* **50**(14), 4860–4878 (2015)
83. F. Zhang, M. Reich, O. Kessler, E. Burkel, The potential of rapid cooling spark plasma sintering for metallic materials. *Mater. Today* **16**(5), 192–197 (2013)
84. A. Azarniya, S. Sovizi, A. Azarniya, M.R.R.T. Boyuk, T. Varol, P. Nithyadharseni, H.R.M. Hosseini, S. Ramakrishna, M.V. Reddy, Physicomechanical properties of spark plasma sintered carbon nanotube-containing ceramic matrix nanocomposites. *Nanoscale* **9**(35), 12779–12820 (2017)
85. V.N. Chuvildeev, D.V. Panov, M.S. Boldin, A.V. Nokhrin, Y.V. Blagoveshchensky, N.V. Sakharov, S.V. Shotin, D.N. Kotkov, Structure and properties of advanced materials obtained by spark plasma sintering. *Acta Astronaut.* **109**, 172–176 (2015)
86. Z.H. Zhang, Z.F. Liu, J.F. Lu, X.B. Shen, F.C. Wang, Y.D. Wang, The sintering mechanism in spark plasma sintering—proof of the occurrence of spark discharge. *Scr. Mater.* **81**, 56–59 (2014)
87. H.C. Oh, S.H. Lee, S.C. Choi, The reaction mechanism for the low temperature synthesis of Cr₂AlC under electronic field. *J. Alloys Compd.* **587**, 296–302 (2014)
88. M. Tokita, The potential of spark plasma sintering (SPS) method for the fabrication on an industrial scale of functionally graded materials, in *Advances in Science and Technology*, vol. 63, (Trans Tech Publications Ltd., 2010), pp. 322–331
89. P. Wang, J. Song, M.L.S. Nai, J. Wei, Experimental analysis of additively manufactured component and design guidelines for lightweight structures: A case study using electron beam melting. *Addit. Manuf.* **33**, 101088 (2020)
90. S. Dizdar, Y. Lyu, C. Lampa, U. Olofsson, Grey cast iron brake discs laser clad with nickel-tungsten carbide—Friction, wear and airborne wear particle emission. *Atmos.* **11**(6), 621 (2020)
91. G.H. Wang, Y.X. Li, Thermal conductivity of cast iron—A review. *China Found* **17**(2), 85 (2020)
92. U. Neveling, Palabora mining company annual report on ambient air quality monitoring, 2011
93. D.O. Okanigbe, Production of copper and copper oxide nano-particles from leach solution of low grade copper smelter dust, 2019
94. D.O. Okanigbe, A.P.I. Popoola, A.A. Adeleke, Characterization of copper smelter dust for copper recovery. *Proc. Manuf* **7**, 121–126 (2017)
95. J.E. Duffy, *Modern Automotive Technology* (The Goodheart-Willcox Company. INC, Tinley Park, 2004)
96. H. Attar, M.J. Birmingham, S. Ehtemam-Haghighi, A. Dehghan-Manshadi, D. Kent, M.S. Dargusch, Evaluation of the mechanical and wear properties of titanium produced by three different additive manufacturing methods for biomedical application. *Mater. Sci. Eng. A* **760**, 339–345 (2019)
97. A. Woźniak, M. Adamiak, G. Chladek, M. Bonek, W. Walke, O. Bialas, The influence of hybrid surface modification on the selected properties of CP titanium grade II manufactured by selective laser melting. *Materials* **13**(12), 2829 (2020)
98. V. Vaithyanathan, V. Balasubramanian, S. Malarvizhi, V. Petley, S. Verma, Establishing relationship between fusion zone hardness and grain size of gas tungsten constricted arc welded thin sheets of titanium alloy. *SN Appl. Sci* **2**(1), 1–12 (2020)
99. D.P. Yan, X. Jin, Characterization of shear band formation and microstructure evolution during orthogonal cutting of Ti-5553: Part I—Shear angle, strain and strain rate. *J. Mater. Eng. Perform.* **29**, 1–12 (2020)
100. A. Hadadian, R. Sedaghati, Analysis and design optimization of double-sided deep cold rolling process of a Ti-6Al-4V blade. *Int. J. Adv. Manuf. Technol.* **108**, 2103–2120 (2020)
101. G. Lütjering, J.C. Williams, Alpha + Beta alloys, in *Titanium*, (Springer, 2003) https://doi.org/10.1007/978-3-540-71398-2_5
102. P. Fonda, Z. Wang, K. Yamazaki, Y. Akutsu, A fundamental study on Ti-6Al-4V's thermal and electrical properties and their relation to EDM productivity. *J. Mater. Process. Technol.* **202**(1–3), 583–589 (2008)

103. F. Borgioli, E. Galvanetto, F. Iozzelli, G. Pradelli, Improvement of wear resistance of Ti-6Al-4V alloy by means of thermal oxidation. *Mater. Lett.* **59**(17), 2159–2162 (2005)
104. O.E. Falodun, B.A. Obadele, S.R. Oke, O.O. Ige, P.A. Olubambi, M.L. Lethabane, S.W. Bhero, Influence of spark plasma sintering on microstructure and wear behaviour of Ti-6Al-4V reinforced with nanosized TiN. *Trans. Nonferrous Metals Soc. China* **28**(1), 47–54 (2018)
105. G.E.R.D. Lütjering, Influence of processing on microstructure and mechanical properties of ($\alpha + \beta$) titanium alloys. *Mater. Sci. Eng. A* **243**(1–2), 32–45 (1998)
106. R. Yazdi, H.M. Ghasemi, M. Abedini, C. Wang, A. Neville, Oxygen diffusion layer on Ti-6Al-4V alloy: Scratch and dry wear resistance. *Tribol. Lett.* **67**(4), 1–15 (2019)
107. Y.R. Choi, S.D. Sun, Q. Liu, M. Brandt, M. Qian, Influence of deposition strategy on the microstructure and fatigue properties of laser metal deposited Ti-6Al-4V powder on Ti-6Al-4V substrate. *Int. J. Fatigue* **130**, 105236 (2020)
108. G. Martino, U.S. Patent Application No. 16/104,659, 2019
109. J. Qu, P.J. Blau, B.C. Jolly, Oxygen-diffused titanium as a candidate brake rotor material. *Wear* **267**(5–8), 818–822 (2009)
110. G.P. Burns, Titanium dioxide dielectric films formed by rapid thermal oxidation. *J. Appl. Phys.* **65**(5), 2095–2097 (1989)
111. C. Boettcher, First prize deep case hardening of titanium alloys with oxygen. *Surf. Eng.* **16**(2), 148–152 (2000)
112. H. Dong, A. Bloyce, P.H. Morton, T. Bell, Surface engineering to improve tribological performance of Ti-6Al-4V. *Surf. Eng.* **13**(5), 402–406 (1997)
113. A.S. Patil, V.D. Hiwarkar, P.K. Verma, R.K. Khatirkar, Effect of TiB₂ addition on the microstructure and wear resistance of Ti-6Al-4V alloy fabricated through direct metal laser sintering (DMLS). *J. Alloys Compd.* **777**, 165–173 (2019)
114. N. Saunders, Modelling of phase equilibria in Ti-alloys, in *Titanium'95- Science and Technology*, Vol. 3, pp. 2167–2176 (1996)
115. F.H. Gordon, S.P. Turner, R. Taylor, T.W. Clyne, The effect of the interface on the thermal conductivity of titanium-based composites. *Composites* **25**(7), 583–592 (1994)
116. V.I. Kushch, Numerical algorithm of multipole expansion method for conductivity of ellipsoidal particle composite. *J. Comput. Phys.* **418**, 109642 (2020)
117. B.M. Kim, Y.K. Cho, S.Y. Yoon, R. Stevens, H.C. Park, Mullite whiskers derived from kaolin. *Ceram. Int.* **35**(2), 579–583 (2009)
118. S.G. Tabrizi, S.A. Sajjadi, A. Babakhani, W. Lu, Influence of spark plasma sintering and subsequent hot rolling on microstructure and flexural behavior of in-situ TiB and TiC reinforced Ti-6Al-4V composite. *Mater. Sci. Eng. A* **624**, 271–278 (2015)
119. Y. Quan, F. Zhang, H. Rebl, B. Nebe, O. Kebler, E. Burkel, Ti-6Al-4V foams fabricated by spark plasma sintering with post-heat treatment. *Mater. Sci. Eng. A* **565**, 118–125 (2013)
120. A.O. Adegbenjo, B.A. Obadele, P.A. Olubambi, Densification, hardness and tribological characteristics of MWCNTs reinforced Ti6Al4V compacts consolidated by spark plasma sintering. *J. Alloys Compd.* **749**, 818–833 (2018)
121. G.D. Revankar, R. Shetty, S.S. Rao, V.N. Gaitonde, Wear resistance enhancement of titanium alloy (Ti-6Al-4V) by ball burnishing process. *J. Mater. Res. Technol.* **6**(1), 13–32 (2017)
122. J.O. Abe, A.P.I. Popoola, O.M. Popoola, Consolidation of Ti-6Al-4V alloy and refractory nitride nanoparticles by spark plasma sintering method: Microstructure, mechanical, corrosion and oxidation characteristics. *Mater. Sci. Eng. A* **774**, 138920 (2020)
123. P.L. Linda, D.O. Okanigbe, A.P.I. Popoola, O.M. Popoola, Characterization of density separated mullite rich tailings from a secondary copper resource, a potential reinforcement material for development of an enhanced thermally conductive and wear resistant Ti-6Al-4V matrix composite, in *The Proceedings of the 60th International Conference of Metallurgist. Canada*, (2021)